Feasibility Analysis of the Installation of a Guided-Wave HEMP Simulator in an Electromagnetic Shielding Room

Yaoyao Li [1], Donglin Su [1*], Shuo Cui [1], and Weimin Li [2]

[1] School of Electronic and Information Engineering
Beihang University, Beijing, 100191, China
bravegoal@126.com, sdl@buaa.edu.cn, cuishuo@buaa.edu.cn

[2] China Academy of Launch Vehicle Technology, CALT
No. 1 Nan Da Hong Men Road, Fengtai District, Beijing, 100076, China
liweimin8103@163.com

Abstract ─ Field strength, waveform and uniformity are crucial to the validity of high-altitude electromagnetic pulse (HEMP) radiation sensitivity test (RS05/RS105) for large transient field facilities which are placed in expensive semi-anechoic chambers (SAC) usually. In this paper, we present a type of space requirements of those large transient field facilities installations in cheaper electromagnetic shielding room (ESR) by quantitative simulation analysis of the crucial factors. The field uniformity and the accuracy of guided-wave EMP simulator (GWES) in a SAC are verified by numerical cases and experiments. Time domain finite integral method (FIT) is employed to compute field data and singular value decomposition (SVD) technique has been used to extract the higher order modes (HOM). Based on the validated model, feasibility of GWES installation in an ESR was analyzed. The minimum space requirement of GWES installation has been obtained through optimization.

Index Terms ─ Field uniformity, HEMP, higher order modes, singular value decomposition, transient electromagnetic field.

I. INTRODUCTION

High-Altitude Electromagnetic Pulse (HEMP) is produced by nuclear explosion at high altitude and characterized by intense electric field strength, short duration, wide band in the frequency spectrum and large range coverage, which can damage electronic equipment of radar and communication systems, wires, crystal diodes, transistors, integrated circuits resistors, capacitors, filters, relays and other components [1, 2]. Therefore, the HEMP sensitivity test becomes critical for military and civil electronic systems. HEMP simulators are applied to generate pulse electric field which simulates the early nuclear explosion radiation. The waveforms are specified in MIL-STD-461G for operating RS105 test (transient electromagnetic field radiated susceptibility tests) [3, 4, 5]. In order to obtain good field distribution uniformity, guided-wave EMP simulators are widely used in electromagnetic compatibility (EMC) susceptibility tests of airplanes, vessels and other electronic devices and systems.

Several HEMP simulators satisfying the fast leading-edge requirement of IEC 61000-2-9 were designed and built worldwide, such as ALECS, ARES, EMPRESS II, and SIEM-2. These generators are generally built in open-area test site (OATS) or SAC to avoid affecting the test area. Depending on the size of the EUT, the size of these transient field facilities varies from several meters to several hundred meters. In indoor GWES sites, the low operating frequency (200 MHz) characteristics require ferrite absorbing materials, which is expensive both in space and money. However, if the EM field characteristics of the GWES in the room can be accurately predicted, the local laying of EM absorbing materials can be used and the cost can be significantly reduced. In [6], many HEMP simulator concepts evolved from design are described. In [7]-[9], a summary of developments in the HEMP research worldwide since 1975 was provided. In addition, the radiation patterns, higher order modes and some performance analysis research of HEMP simulators have been presented in [10]-[12]. A field uniformity analysis and calibrate method for eliminating the measurement error is presented in [13], [14]. Besides, in [15]-[16] the basic types or categories of EMP simulators were discussed. All of these works are about the standards, modeling, simulation and performance evaluation of HEMP simulator, without considering the performance changes after installation. No result of this type has been reported in the open literature.

In this paper, feasibility of a GWES placement in an ESR was analyzed. In Section II, we present the GWES computational model and simulation results by CST

Submitted On: October 14, 2018
Accepted On: March 21, 2019

[20]. The field uniformity and the accuracy of the experimental simulator are verified by numerical cases and experiments. We proved that the electric field in the working area of guided wave EMP simulator can be expressed as a linear combination of TEM, TM and TE modes, which is of great importance to the analysis of field uniformity, radiation leakage and fundamental mode damage. In Section III, FIT has been used to compute field data and SVD technique has been employed to extract the HOM on a grid of 7 x 5. In Section IV, we analyzed the influence of metal wall on GWES performance based on the validated model. Feasibility of GWES installation in an ESR was analyzed. The minimum space requirement of GWES installation has been obtained through optimization.

II. GWES MODELING AND VERIFICATION

A. GWES modeling

The modeling process is as follows. Firstly, the structure model and distributed load of HEMP generator were established. Secondly, the boundary condition and the reference point or reference plane were selected. Lastly, the structure and load value of the simulator are optimized to approximate the measured results. The simulation model is shown in Fig. 1. Virtual field probes are utilized in the test zone of the GWES model to perform a complete field mapping. Some parameters used in this study are as follows. The symmetric geometry is 1:1 according to [19] and the size is 5700 mm × 2500 mm ×1800mm. The corresponding rise time is 2.47 ns and 99% energy effective bandwidth is 95.2MHz. The maximum frequency of the simulation is set as 600 MHz, the metal wire grating and the plate are perfect electric conductors, and the single load is 138 ohms. The background environment is assigned to air.

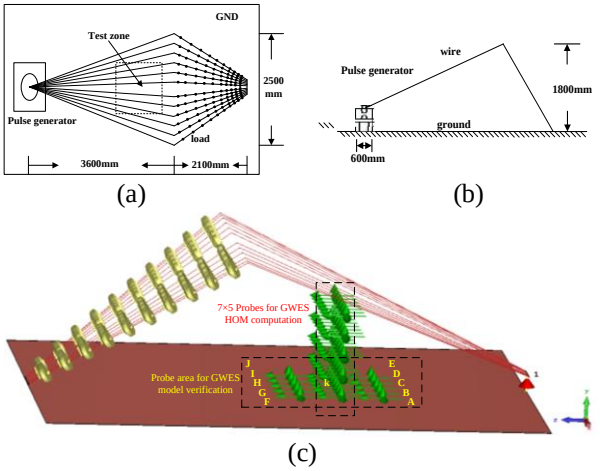

Fig. 1. Geometry of a GWES: (a) top view, (b) side view, and (c) 3-D structure and monitors placement.

The test zone is 1000 mm × 1000 mm. Eleven virtual field probes are placed on the ground plane of the test zone of the GWES model to perform field mapping. The positions of the probes are illustrated in Fig. 1 (c) marked as A to K. Also, there are 7 × 5 probes to monitor the EM field for HOM extracted by SVD.

B. Verification model

An ideal pulse generator voltage source U(t) is applied to produce the standard double exponential pulsed field E(t) [13], which are as follows:

$$U(t)=\begin{cases}0, & \text{when } t\le 0\\ U_0\cdot(e^{-\alpha t}-e^{-\beta t}), & \text{when } t>0\end{cases} \quad (1)$$

$$E(t)=\begin{cases}0, & \text{when } t\le 0\\ E_0\cdot k\cdot(e^{-\alpha t}-e^{-\beta t}), & \text{when } t>0\end{cases} \quad (2)$$

where $U_0=6.5\times10^4\,\mathrm{V}$, $E_0=5\times10^4\,\mathrm{V/m}$, $\alpha=4\times10^7\,\mathrm{s}^{-1}$, $\beta=6\times10^8\,\mathrm{s}^{-1}$, and $k=1.3$.

To verify the GWES model, field uniformity and waveform are compared by simulation and experiment. The measurement setup is shown in Fig. 2. A differential D-dot sensor is used as the ground plane sensor. Thus an integrator has to be used together with the D-dot. The correction factor of the D-dot sensor is 37.4 mV. The relationship between the correction factor C of the sensor, the oscilloscope reading U, and the peak electric field E is demonstrated in (3) [19]:

$$E(KV/m)=U(mV)/C[mV/(kV/m)]. \quad (3)$$

The measurement is as follows: Firstly, the electric field probe is calibrated and then configures the measurement as shown in Fig. 2. Secondly, the voltage is converted into the field strength of the observation point according to (3). Lastly, move the probe to the observation points shown in Fig. 1 in turn, and record readings to complete the measurement.

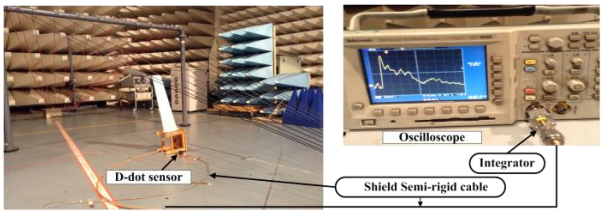

Fig. 2. Measurement setup of the GWES.

The field uniformity of the simulation model is verified as follows. The field uniformity will not change due to the output voltage of GWES. So we picked a median of 20.1 kV as the GWES output voltage to facilitate the test. A time domain FIT method has been employed to compute the time domain field results. We select CST as computational tool. In MWS, the virtual probes can monitor EM field components in the appointed

space position. And we selected peak field as the field uniformity inputs. According to the simulation and measurement position shown in Fig. 1 (c), numerical results and measurement results of the field in different positions are listed in Table 1.

Table 1: Comparison of simulation and measurement results of E-field uniformity

p	OR (mv)	OREY (KV/m)	ORLEY (dBV/m)	SEY (dBV/m)
A	48.0	1.28	62.17	111.236
B	52.4	1.40	62.93	111.326
C	54.8	1.47	63.32	111.481
D	54.4	1.45	63.25	111.394
E	50.2	1.34	62.56	111.053
F	35.6	0.95	59.57	109.876
G	36.4	0.97	59.76	109.938
H	38.4	1.03	60.23	108.442
I	35.0	0.94	59.42	108.386
J	34.8	0.93	59.37	108.205
K	42.8	1.14	61.17	109.82
Field uniformity(dB)		3.9		3.3

Where P represents the position of monitors, OR refers to oscilloscope reading voltage, OREY is the oscilloscope reading voltage transfer to linear field strength, ORLEY shows the oscilloscope reading voltage transfer to Logarithmic field strength, and SEY represents simulation field strength. It is shown that the deviation of the GWES model on field uniformity equals to 0.6dB.

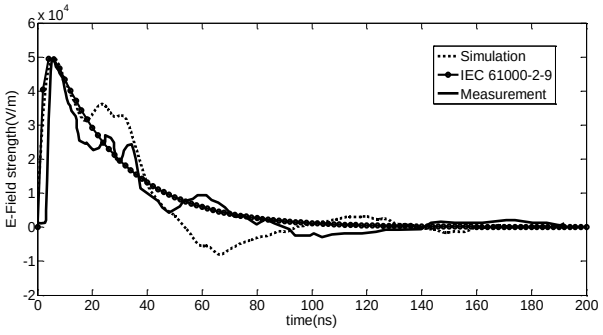

Fig. 3. Comparison of the electric field waveform between IEC 61000-2-9, simulation and measurement.

The field uniformity of eleven points from A to K is shown in Table 1. Without loss of generality, point C marked in Fig. 3 (c) is selected as the reference point for EM field waveform analysis. The numerical simulation result, standard curve and measurement result of point C are shown in Fig. 3. In the measurement, 1 to 3 nanoseconds propagation delay usually occurs when HEMP waveform propagates from MAX voltage source to point C, while there is no delay in the standard and simulation model. Therefore, the simulation result, standard curve and measurement cannot be overlapped in the time domain. In order to verify the accuracy, the rise time and maximum field strength are selected for comparison. The rise time is 2.47 ns and maximum field strength is 50000V/m. It shows good agreement with the HEMP standard of IEC 61000-2-9 [21], which an industry standards for HEMP waveform.

The electric field strength distributions through numerical simulation are shown in Fig. 4. The maximum field strength can reach 50000V/m. Those results show that the experimental GWES meets the standard requirements.

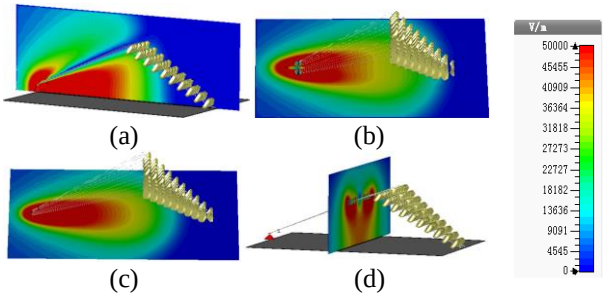

Fig. 4. GWES electric field strength distribution: (a) x=0 mm plane, (b) y=200 mm plane, (c) y= 500mm plane, and (d) Z=2820 mm plane.

The above work shows a good agreement to the EM field waveform, distribution and uniformity with the measured data, which proves that the GWES model is credible.

III. APPLICATION SVD FOR HOM ANALYSIS

A. Singular value decomposition (SVD)

In SVD, a matrix is decomposed into three matrices of same size. In this subsection, we present a brief description of the method and its application to the modal analysis of FIT simulation. The SVD of a matrix A is defined as follows [17, 18]:

If $A \in \Re^{m\times n}$, there would exist orthogonal matrices:

$$U = \left(u_1, u_2, \cdots u_m\right) \in \Re^{m\times m}, \tag{4}$$

$$V = \left(v_1, v_2, \cdots v_m\right) \in \Re^{n\times n}, \tag{5}$$

such that,

$$A = USV^T = \sum_{i=1}^{r} u_i \cdot \alpha_i \cdot v_i^T, \quad r = \min\left\{m, n\right\}, \tag{6}$$

where

$$S = diag\left(\alpha_1, \alpha_2, \cdots \alpha_r\right), \quad \alpha_1 \geq \cdots \geq \alpha_r \geq 0. \tag{7}$$

The vector u_i and v_i denote the *i*th left and right singular vectors, respectively, and the diagonal elements α_i of *S* are the singular values of matrix *A*. Considering a physical quantity simultaneously measured at *m*

different positions and sampled at *n* different times with a sampling interval t_s , the matrix representation of the above observation can be generally expressed by a rectangular array $x_{ij} = x_j\left[(i-1)t_s\right]$, where the row index *i* refers to time and the column index *j* refers to the channel. The SVD of the matrix x_{ij} is expressed as $X_{ij} = U_i^k s_k V_j^k$. The singular values *S* represent the amplitude of a mode, while *U* and *V* are the basis functions. In summary, the matrix X_{ij} has been decomposed into three parts - time (*U*), amplitude (*S*) and space (*V*).

B. SVD analysis on computed result

Based on the verified GWES model. FIT has been used to compute field data and SVD technique has been used to extract the higher order modes. SVD is performed on $E(x_{ij})$ measured at 35 positions (z=2320 mm plan) as shown in Fig. 1 (c). These field monitors locates in the y direction with an interval of 0.8 m. Each channel records 1000 points with a sampling interval of 200 ns.

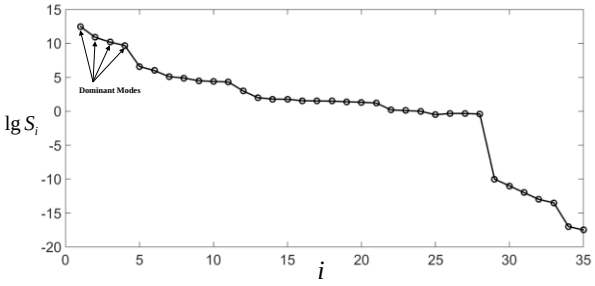

Fig. 5. Logarithms of the singular value S_i

The 35 singular values of the decomposed components are shown in Fig. 5. The x axis represents observation position indexes. Following the principle of [17], the word "dominant" is used in an approximate sense to describe modes whose singular values lie within three orders of magnitude of the strongest mode. It shows that there are four dominant modes (Eigen modes).

Figures 6 (a)-(d) exhibit the eigenvectors in the descending order. The eigen vector in Fig. 6 (a) is almost constant. Obviously, it corresponds to the TEM mode, which does not have any zero crossing. The eigen vectors illustrated in Figs. 6 (a), (b), (c) and (d) have one, two or three zero crossing, respectively, which represent the TM0 (TEM), TM1, TM2 and TM3 modes respectively.

The above HOM will cause the radiation leakage and destructive of the fundamental mode. In the following parts, we will analysis the radiation leakage in an ESR, and its impact to the test zone.

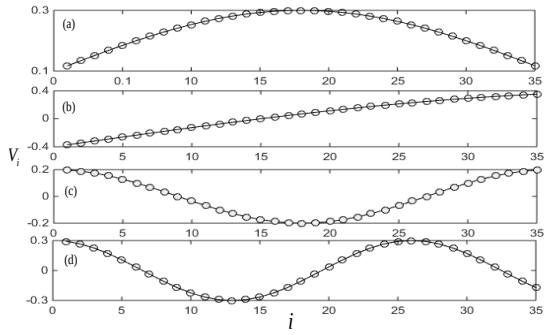

Fig. 6. Eigen vectors of the dominant modes.

IV. GWES PLACEMENT IN AN ESR

Limited by the funding, the indoor GWES test facility cannot have full coverage by absorbing materials. The size of a research institution ESR is shown in Fig. 7.

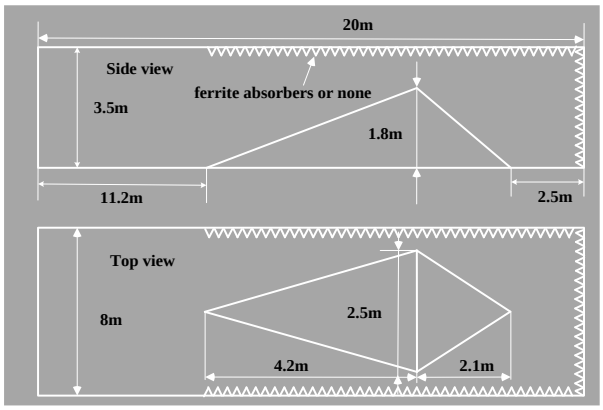

Fig. 7. An indoor GWES site.

If metallic walls (or electrical installations, barriers, etc.) are in the vicinity of the installation site, reflections of the wave can occur. The reflected waves will return to the test zone and added to the field below the antenna. Depending on the phase of the reflected wave, the distortion of the signal could be positive or negative. In order to analyze the feasibility, we carry out a simulation analysis based on the validated simulator above mentioned. It is assumed that absorbing materials forms a perfectly matched layer. The analysis procedure is shown in Fig. 8.

Step 1): Establish a model of shielding chamber loading GWES according to the actual size of ESR.

Step 2): The load surface wall, along with the front, rear and top walls are set as metal surfaces, while other walls are set as open. The distribution of the simulated field and the waveform characteristics of the uniform field in the test area are compared with those in the fully open condition, and the influential wall is obtained.

Step 3): If the influential wall exists, the part of the wall with larger influential surface is set as open, and the other area is metal wall. The minimum space requirement is obtained by the simulation method of step 2.

Step 4): The site size requirement of the test GWES is formed to provide technical support for MIL-STD-461G.

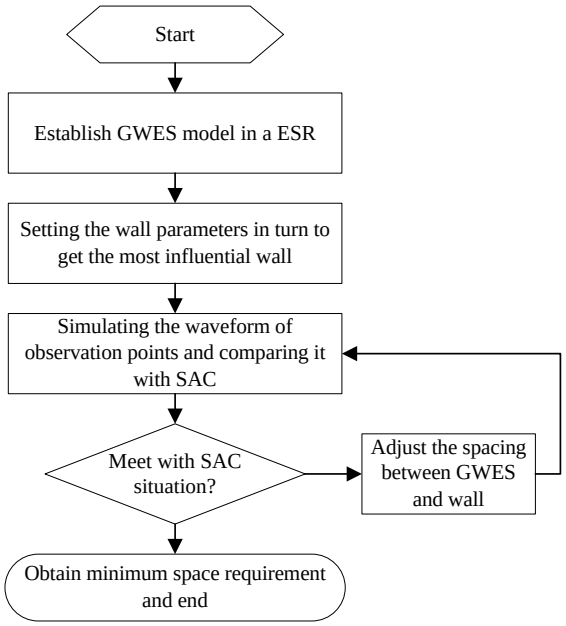

Fig. 8. Proposed installation feasibility analysis method operating flow chart.

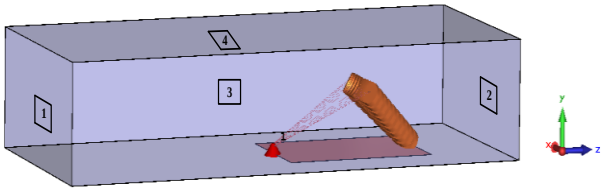

Fig. 9. GWES installation in an ESR model

The GWES-ESR model is shown in Fig. 9. The GWES model which is depicted in Fig. 9 is the same as we stated in part II. We choose the most important parameters of the E1 shape, i.e., the rise time $\tau_{10\%\sim90\%}$, the pulse width at half maximum t_f and the peak amplitude of the electric field E_0 [2] as the index of feasibility evaluation.

Comparing Fig. 10 (a) with Fig. 10 (b), it can be observed that field distributions produced by GWES installation in ESR and SAC situations are the same in the test zone which is 1000 mm × 1000 mm ×1000mm as shown in Fig. 1 (a). Shielding room slightly enhances the indoor field strength, compared to SAC. The field uniformity does not change according to the same calculation method in Table 1.

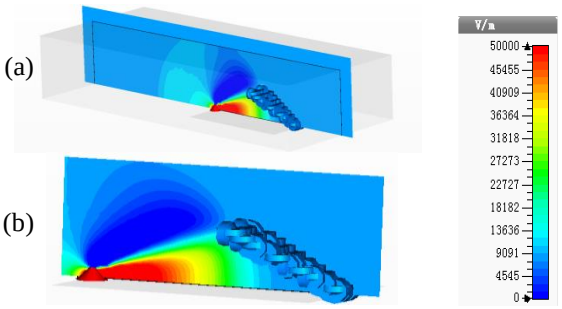

Fig. 10. Field distributions at x=0 mm plane and t=8.5ns produced by GWES installation in ESR and SAC situations.

In order to get the influence of shielding room on the test system, the waveform comparison between shielding room and semi-anechoic chambers at K point as illustrated in Fig. 1 (c) is carried out. The result is shown in Fig. 11.

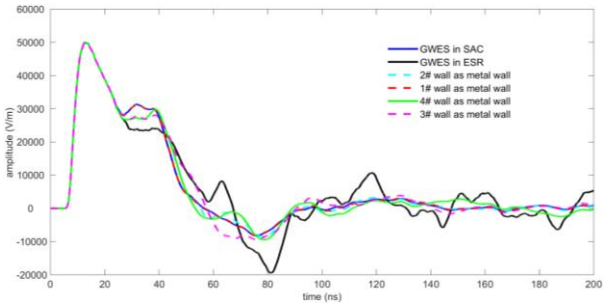

Fig. 11. Field waveforms produced by GWES installation in SAC and ESR situations

Considering Fig. 11 and the calculation results, it can be found that $\tau_{10\%\sim90\%}$, t_f and E_0 in ESR are almost the same with those from SAC condition. However, the electric field waveform in the back edge is distorted because of severe oscillatory effect from the reflection of the wall appears on the back edge of the pulse. To assess that impact, we select 5000 points to calculate the mean error between five curves and SAC curves. As shown in Table 2, installation in ESR and 4# wall has the greatest impact.

Table 2: Comparison of mean error on different simulation situation

Simulation Situation	Mean Error (V/m)
GWES in ESR	4276
2# wall as metal wall	285
1# wall as metal wall	182
4# wall as metal wall	1242
3# wall as metal wall	120

To eliminate the damped oscillation effect in the back edge caused by wall, we optimized the minimum distance between the facility and the wall. We define d1, d2, d3, whose shown on Fig. 12 are the variables to be optimized. We select the average deviation of E_z, E_x and E_y on pulse delay amplitude for SAC and ESR as the objective goal, so as to optimize d1, d2 and d3 respectively. When the average deviation of E_z is less than 10V/m, d1 is obtained. When the average deviation of E_x is less than 10V/m, d2 is obtained. When the average deviation of E_y is less than 10V/m, d3 is obtained. As shown on Fig. 11, the damped oscillation effect is minimum when d1 is equal to 3.2m, d2 is equal to 1.5m and d3 is equal to 1.8*H. It is feasible to install the GWES in ESR as long as the specified space requirements are followed.

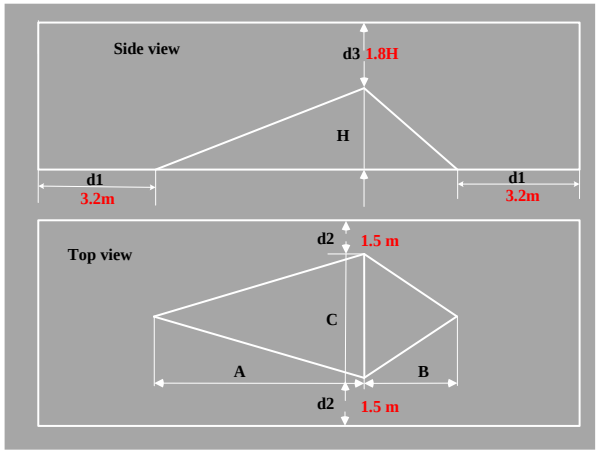

Fig. 12. The optimized minimum space requirements of GWES installation.

V. CONCLUSION

In this paper, feasibility of a popular guided-wave EMP simulator placement in an electromagnetic shielding room was analyzed by time domain finite integral method and singular value decomposition. A GWES model is built and validated by the good agreement on field strength, waveform and uniformity between simulations and measurements. Based on this GWES model, FIT has been used to compute field data and the SVD technique has been used to extract the higher order modes. Waveform distortion of GWES in ESR was simulated by FIT and the feasibility of GWES installation in an ESR was further analyzed. This proves that installation of the GWES in ESR as long as the specified space requirements is feasible and the minimal space requirement of GWES installation has been given by optimization method.

ACKNOWLEDGMENT

This work was supported by the project 61427803 and 61521019 from the National Natural Science Foundation of China (NSFC).

REFERENCES

[1] S. Song, H. Jiang, and Y.-L. Huang, "Simulation and analysis of HEMP coupling effect on a wire inside an apertured cylindrical shielding cavity," *Appl. Comput. Electromagn. Soc. J.*, vol. 27, no. 6, pp. 505-515, June 2012.

[2] F. Sabath and S. Potthast, "Tolerance values and the confidence level for high-altitude electromagnetic pulse (HEMP) field tests," *IEEE Trans. Electromagn. Compat.*, vol. 55, no. 3, pp. 518-525, June 2013.

[3] *Requirements for the control of electromagnetic interference characteristics of subsystems and equipment*, MIL-STD-461G, Dec. 2015.

[4] *Electromagnetic Compatibility (EMC) — Part 4-32: Testing and Measurement Techniques —High-Altitude Electromagnetic Pulse (HEMP) Simulator Compendium*, IEC 61000-4-32:2002, 2002.

[5] R. Hoad and W. A. Radasky, "Progress in high-altitude electromagnetic pulse (HEMP) standardization," *IEEE Trans. Electromagn. Compat.*, vol. 55, no. 3, pp. 532-538, June 2013.

[6] W. D. Prather and D. V. Giri, "Early developments in sensors and simulators at the air force weapons laboratory," *IEEE Trans. Electromagn. Compat.*, vol. 55, no. 3, pp. 431-439, June 2013.

[7] M. Ianoz, "A review of HEMP activities in Europe (1970 – 1995)," *IEEE Trans. Electromagn. Compat.*, vol. 55, no. 3, pp. 412-421, June 2013.

[8] J. C. Giles and W. D. Prather, "Worldwide high-altitude nuclear electromagnetic pulse simulators," *IEEE Trans. Electromagn. Compat.*, vol. 55, no. 3, pp. 475-483, June 2013.

[9] L. Shi, X. Zhang, Z. Sun, and R. Ma, "An overview of the HEMP research in China," *IEEE Trans. Electromagn. Compat.*, vol. 55, no. 3, pp. 422-430, June 2013.

[10] R. Kichouliya and M. J. Thomas, "Radiation pattern of a hybrid type high altitude electromagnetic pulse (HEMP) simulator," *IEEE International Symposium on Electromagnetic Compatibility*, Ottawa, pp. 530-535, July 2016.

[11] R. Kichouliya, S. M. Satav, and M. J. Thomas, "Experimental investigation on higher order modes in guided wave high altitude electromagnetic pulse (HEMP) simulator," *IEEE International Symposium on Electromagnetic Compatibility*, Ottawa, pp. 153-158, July 2016.

[12] J. J. A. Klaasen, "An efficient method for the

performance analysis of bounded-wave nuclear EMP simulators," *IEEE Trans. Electromagn. Compat.*, vol. 35, no. 3, pp. 329-338, Aug. 1993.

[13] L. Yao, T. Shen, N. Kang, J. Huang, D. Liu, F. Zhang, and H. Sun, "Use of a reference point method to calibrate the field uniformity when testing with transient electromagnetic fields," *IEEE Trans. Electromagn. Compat.*, vol. 59, no. 2, pp. 352-357, Apr. 2017.

[14] L. Yao, T. Shen, N. Kang, D. Liu, and J. Huang, "Time-domain simulation and measurement of a guided-eave EMP simulator's field uniformity," *IEEE Trans. Electromagn. Compat.*, vol. 55, no. 6, pp. 1187-1194, Dec. 2013.

[15] C. E. Baum, "EMP simulators for various types of nuclear EMP environments: An interim categorization," *IEEE Trans. Electromagn. Compat.*, vol. 20, no. 1, pp. 35-53, Dec. 1978.

[16] D. V. Giri, C. E. Baum, and W. D. Prather, "The relationship between NEMP standards and simulator performance specifications," *Sensor Simulation Note 538 Idus Martiae*, 2009.

[17] S. Ahmed and E. Li, "Application of singular value decomposition on FDTD simulation results – A novel approach for modal analysis of complex electromagnetic problems," *IEEE Microwave and Wireless Components Letters*, vol. 14, no. 11, pp. 519-521, Nov. 2004.

[18] S. Ahmed, D. Raju, S. Caturvedi, and R. Jha, "Modal analysis for a bounded wave simulator – Part I: Effect of test objects," *IEEE Trans. Electromagn. Compat.*, vol. 47, no. 1, pp. 171-182, Feb. 2005.

[19] *NEMP Transient Pulse Simulator Installation and User's Manual*, Montenaemc sa, Switzerland.

[20] CST STUDIO SUITE™ 2011, CST AG, Germany. www.cst.com

[21] Compatibility E. Part 2: Environment— Section: Description of HEMP Environment—Radiated Disturbance, *IEC 61000-2-9 Ed. 1.0*, Feb. 1996.

Yaoyao Li was born in Jingzhou, China, in 1986. He received the Ph.D. degree in Electromagnetic Compatibility and Electromagnetic Environment in 2017 from Beihang University, Beijing, China. His current research interests include System level electromagnetic compatibility and electromagnetic protection.

Donglin Su received the B.S., M.S., and Ph.D. degrees in Electrical Engineering from Beihang University, Beijing, China, in 1983, 1986, and 1999, respectively.

In 1986, she joined the Faculty of School of Electronics and Information Engineering, BUAA, where she was first an Assistant, then a Lecturer, later on an Associate Professor, and is currently a Full Professor. From 1996 to 1998, she was a Visiting Scholar with the Department of Electrical Engineering, University of California, Los Angeles (UCLA), Los Angeles, CA, USA, under the BUAA–UCLA Joint Ph.D. Program. She has authored more than 100 papers and coauthored several books. Her research interests include the numerical methods for microwave and millimeter-wave integrated circuits and systematic electromagnetic compatibility design of various aircrafts. Su is a Senior Member of the Chinese Institute of Electronics. She is the Chair of Beijing Chapter of the IEEE Antennas and Propagation Society and the Deputy Chair of the Antennas Society, Chinese Institute of Electronics. She was a recipient of two National Awards for Science and Technology Progress in 2007 and 2012, respectively

Shuo Cui was born in Qinhuangdao, China, in 1993. She received the B.E. degree in Applied Physics from Beihang University, Beijing, China, where she is currently working toward the Ph.D. degree in Electromagnetic Compatibility and Electromagnetic Environment. Her current research interests include electromagnetic emission and Electromagnetic calculation.

Weimin Li was born in Taiyuan, China, in 1981. She received the Ph.D. degree in Circuits and Systems in 2012 from Beihang University. He is currently a Senior Engineer with China Academy of Launch Vehicle Technology, Beijing, China. His research focuses on electromagnetic compatibility test.